CHEMISTRY OF MATERIALS

Synthesis, Structures, and Magnetic Properties of Rare-Earth Cobalt Arsenides, RCo_2As_2 (R = La, Ce, Pr, Nd)

Corey M. Thompson,[†] Xiaoyan Tan,[†] Kirill Kovnir,[†] V. Ovidiu Garlea,[‡] Andrei A. Gippius,[§] Alexander A. Yaroslavtsev,[∥,⊥,#] Alexey P. Menushenkov,[∥] Roman V. Chernikov,[∇] Norbert Büttgen,[○] Wolfgang Krätschmer,[○] Yan V. Zubavichus,[□] and Michael Shatruk*[,†]

[†]Department of Chemistry and Biochemistry, Florida State University, Tallahassee, Florida 32306, United States

[‡]Quantum Condensed Matter Division, Oak Ridge National Laboratory, Oak Ridge, Tennessee 37831, United States

[§]Department of Physics, Moscow State University, 119991, Moscow, Russia

[∥]National Research Nuclear University “Moscow Engineering Physics Institute”, 115409 Moscow, Russia

[⊥]European XFEL GmbH, 22761 Hamburg, Germany

[#]Institut für Theoretische Physik, Universität Hamburg, 20355 Hamburg, Germany

[∇]DESY Photon Science, 22603 Hamburg, Germany

[○]Experimental Physics V, University of Augsburg, 86159, Augsburg, Germany

[□]National Research Centre “Kurchatov Institute”, 123182 Moscow, Russia

Ⓢ *Supporting Information*

ABSTRACT: Four rare-earth cobalt arsenides, RCo_2As_2 (R = La, Ce, Pr, Nd), were obtained by reactions of constituent elements in molten Bi. The use of Bi flux also allowed the growth of representative single crystals. All compounds are isostructural and belong to the $ThCr_2Si_2$ type (space group $I4/mmm$). The formation of Co vacancies is observed in all structures, while the structures of La- and Ce-containing compounds also show incorporation of minor Bi defects next to the R crystallographic site. Correspondingly, the general formula of these materials can be written as $R_{1-x}Bi_xCo_{2-\delta}As_2$, with x/δ = 0.03/0.1, 0.05/0.15, 0/0.2, and 0/0.3 for R = La, Ce, Pr, and Nd, respectively. All compounds exhibit high-temperature ferromagnetic ordering of Co magnetic moments in the range 60−200 K. Electronic band structure calculations revealed a high peak in the density of states at the Fermi level, thus supporting the itinerant nature of magnetism in the Co sublattice. The magnetic ordering in the lanthanide sublattice takes place at lower temperatures, with the R moments aligning antiparallel to the Co moments to give a ferrimagnetic ground state. The measurements on oriented single crystals demonstrated significant magnetic anisotropy in the ferrimagnetic state, with the preferred moment alignment along the c axis of the tetragonal lattice. Neutron powder diffraction failed to reveal the structure of magnetically ordered states but confirmed the presence of Co vacancies. X-ray absorption near-edge structure spectroscopy on $Ce_{1.95}Bi_{0.05}Co_{1.85}As_2$ showed the average oxidation state of Ce to be +3.06. Solid state NMR spectroscopy revealed a substantially reduced hyperfine field on the Co atoms in the vicinity of Bi defects.

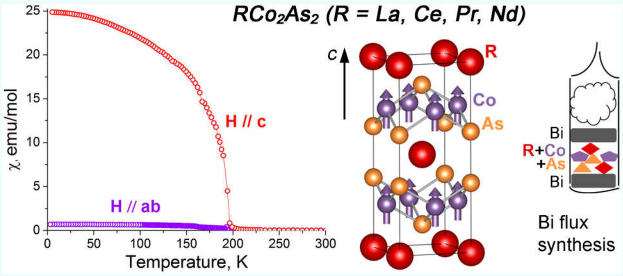

■ INTRODUCTION

Layered pnictides of the $ThCr_2Si_2$ structure type have drawn increasing attention due to the recent discovery of a new class of high-temperature superconductors derived from AFe_2As_2 (A = Ca, Sr, Ba, Eu).[1] The superconductivity is imparted by proper electron- or hole-doping of these parent materials. For example, the substitution of K for Ba or Co for Fe suppresses antiferromagnetic (AFM) ordering in $BaFe_2As_2$ and results in the superconducting behavior with T_C = 38 K in $Ba_{0.6}K_{0.4}Fe_2As_2$[2] and T_C = 22 K in $BaFe_{1.8}Co_{0.2}As_2$.[3] At higher doping levels, the superconductivity disappears and, for instance, pure $BaCo_2As_2$ shows paramagnetic properties.[4]

Naturally, such studies of electron doping in AFe_2As_2 have sparked interest in the Co-containing analogues, ACo_2As_2. Similar to $BaCo_2As_2$, $SrCo_2As_2$ is a paramagnet but shows AFM spin fluctuations at 5 K,[5] while $CaCo_2As_2$ exhibits AFM ordering at ∼70 K.[6] In $EuCo_2As_2$, the AFM ordering occurs at 39 K but it has been attributed to the ordering of the Eu^{2+} $4f$ magnetic moments rather than the Co $3d$ moments.[7] We find, however, that with the exception of $EuCo_2As_2$, very little is

Received: April 28, 2014
Revised: May 16, 2014
Published: May 21, 2014

dx.doi.org/10.1021/cm501522v | Chem. Mater. 2014, 26, 3825−3837

known about the synthesis and properties of other rare-earth containing RCo_2As_2 materials.

The investigation of RCo_2As_2 phases is interesting from the magnetism point of view, considering the rich and fascinating magnetic behavior established for isostructural RCo_2P_2. Among the latter, $LaCo_2P_2$ orders ferromagnetically (FM) at 132 K while other RCo_2P_2 (R = Ce, Pr, Nd, Sm) exhibit AFM ordering above room temperature.[8] Upon doping of Pr (or Nd) for La in $LaCo_2P_2$, the FM ordering temperature increases from 132 to 275 K.[9] Furthermore, the quaternary $La_{1-x}Pr_xCo_2P_2$ phases exhibit multiple magnetic transitions that are not observed in their ternary congeners. For example, as the temperature is lowered, $La_{0.75}Pr_{0.25}Co_2P_2$ undergoes FM ordering of Co 3*d* moments in the *ab* plane of the tetragonal lattice at 170 K, followed by FM ordering of Pr 4*f* moments along the *c* axis at 67 K that causes reorientation of the Co moments along the *c* axis in the direction antiparallel to the Pr moments.[10] Thus, $La_{0.75}Pr_{0.25}Co_2P_2$ is characterized by a ferrimagnetic (FiM) ground state, not observed in any of the ternary RCo_2P_2 phases. Such drastic change in the magnetic behavior upon partial isoelectronic substitution of Pr for La is explained by the stabilization of the ferromagnetism in the Co sublattice due to subtle changes of the electronic structure at the Fermi level.[9]

We also have shown that the substitution of Fe for Co in $LaCo_2P_2$ leads to the suppression of FM ordering and emergence of a spin-glass state even at low concentrations of Fe (~10%).[11] The influence of the pnictogen on the magnetic properties of these materials has been unknown until recently, mainly due to the lack of a reliable synthetic approach to phase-pure RCo_2As_2 samples or their representative single crystals. In fact, prior to our work, there existed only one report on the preparation of RCo_2As_2 in which the attempts to obtain single crystals from Sn flux were unsuccessful.[12]

Recently, we have reported the successful preparation of single-phase $LaCo_2As_2$ and the growth of corresponding single crystals by carrying out the reaction between constituent elements in molten Bi.[13] Similar to $LaCo_2P_2$, which orders FM at T_C = 132 K, $LaCo_2As_2$ shows FM ordering at $T_C \sim 200$ K. Furthermore, we established that a small amount of Bi substitutes for La with a simultaneous formation of vacancies in the Co sublattice, a structural feature not observed for RCo_2P_2 analogues. Herein, we demonstrate that the reaction in Bi flux serves as the general method for the preparation of other RCo_2As_2 materials. We also show that the crystal structures and magnetic behavior of these arsenides are distinctly different from the properties of the corresponding phosphides.

■ MATERIALS AND METHODS

Starting Materials. Finely dispersed powders of lanthanum (99.9%), praseodymium (99.9%), and arsenic (99.99%), as well as bismuth granules (99.997%), were obtained from Alfa Aesar and used as received. Cerium and neodymium filings were obtained from a metal chunk (Michigan Chemical Corporation, 99.9%) stored under oil, which was washed away with dry and air-free hexanes before filing. Cobalt powder (Alfa Aesar, 99.5%) was additionally purified by heating under a flow of H_2 gas at 775 K for 5 h. All manipulations during sample preparation were carried out in an argon-filled drybox (content of O_2 < 1 ppm).

Synthesis. The starting materials were mixed in the R/Co/As/Bi = 1:2:2:30 ratio (total mass = 5 g; R = La, Ce, Pr, Nd) and loaded into 10 mm inner diameter (i.d.) fused silica tubes, which were sealed under vacuum ($<10^{-2}$ mbar). The mixtures were annealed at 1173 K for 10 days and quenched into water. The Bi flux was removed by soaking the samples in a mixture of glacial acetic acid and 30% aqueous H_2O_2 (1:1 v/v) for 2−3 days, followed by washings with dilute HCl (1:1 v/v) and water. The phase purity of samples with R = La, Ce, Pr was confirmed by powder X-ray diffraction, but the sample with R = Nd contained significant amount of impurities. The samples for neutron powder diffraction experiments were prepared by scaling up the total sample mass to 25 g (of which 23.5 g was Bi flux) and using larger silica tubes with 15 mm i.d. The scale-up also led to the formation of larger (~1 × 1 × 0.2 mm^3) single-crystals of RCo_2As_2 which were selected for magnetic property measurements.

General Characterization Methods. Powder X-ray diffraction was performed on a Rigaku DMAX 300 Ultima III powder X-ray diffractometer using Cu Kα radiation (λ = 1.54185 Å) and on an original X-ray diffraction setup using Guinier camera 670 with a Huber imaging plate and a Ge crystal monochromator (Cu Kα_1, λ = 1.54060 Å). For the accurate refinement of the unit cell, elemental Ge was used as an internal standard. The unit cell parameters were calculated by least-squares fitting with the WinCSD software package.[14] Elemental analysis of select single crystals was carried out on a JEOL 5900 scanning electron microscope with an energy-dispersive X-ray (EDX) microanalysis. Magnetic measurements were performed on polycrystalline samples and single crystals with a Quantum Design SQUID magnetometer MPMS-XL. DC magnetic susceptibility measurements were carried out in an applied field of 1 mT in the temperature range 1.8−300 K. Isothermal field dependences of magnetization and hysteresis were measured with the magnetic field varying between −7 and 7 T.

Single Crystal X-ray Diffraction. For the room-temperature experiment, a single crystal was glued with epoxy cement on the tip of a quartz fiber and mounted on a goniometer head of a Bruker AXS SMART diffractometer equipped with an APEX-II CCD detector. The data sets were recorded as ω-scans in steps of 0.3° and integrated with the Bruker SAINT software.[15] All the data sets were indexed in the tetragonal body-centered unit cell. The only systematic extinctions observed corresponded to the *I*-centered lattice. An analytical absorption correction was applied using face-indexing of the crystal. Solution and refinement of the crystal structures was carried out using the SHELX software.[16] The structures were solved in the $I4/mmm$ space group (No. 139), and the final refinement was performed with anisotropic atomic displacement parameters for Co and As atoms. The disordered Bi and R (R = La, Ce) atomic positions were refined isotropically but constrained to have equal atomic displacement parameters. A summary of pertinent information relating to unit cell parameters, data collection, and refinements are provided in Table 1.

Powder Neutron Diffraction. Powder neutron diffraction experiments on $R_{1-x}Bi_xCo_{2-\delta}As_2$ (R = La, Ce) were carried out using the HB-2A high-resolution neutron powder diffractometer at the High Flux Isotope Reactor at Oak Ridge National Laboratory. The λ = 1.536 Å monochromatic radiation was provided by a vertically focusing Ge (115) monochromator. Measurements were performed on a sample of ~3 g held in a cylindrical vanadium container placed in a top-loading closed cycle refrigerator, covering a temperature range 4−300 K. The data were collected by scanning the detector array consisting of 44 ^{3}He tubes in two segments, to cover the total 2θ range 7°−133° in steps of 0.05°. Overlapping detectors for the given step served to average the counting efficiency of each detector. More details about the HB-2A instrument and data collection strategies can be found in the original publication.[17] Rietveld refinement of the collected data was carried out using FULLPROF software.[18]

X-ray Absorption Near-Edge Structure (XANES) Spectroscopy. XANES spectra were measured at L_3-R absorption edges in the transmission mode. Spectra at room temperature and in the range 10−100 K were measured at the beamline "Structural Materials Science" of Kurchatov synchrotron radiation source (Moscow, Russia). Spectra at ~86 K were obtained at the beamline mySpot of BESSY-II storage ring (HZB, Berlin, Germany). The exact value of Ce valence was extracted from the experimental spectra using the conventional fitting with the combination of Lorentz and arctangent curves.

Solid-State NMR Spectroscopy. Field-sweep NMR and zero-field NMR measurements were performed in the 4.6−300 K

Table 1. Data Collection and Structure Refinement Parameters for $R_{1-x}Bi_xCo_{2-\delta}As_2$ (R = La, Ce, Pr, Nd)[a]

compd.[b]	$La_{0.97(1)}Bi_{0.03(1)}Co_{1.91(1)}As_2$	$Ce_{0.95(1)}Bi_{0.05(1)}Co_{1.83(1)}As_2$	$PrCo_{1.78(1)}As_2$	$NdCo_{1.71(1)}As_2$
temp., K	293	293	293	293
λ, Å	0.710 73	0.710 73	0.710 73	0.710 73
space group	$I4/mmm$	$I4/mmm$	$I4/mmm$	$I4/mmm$
unit cell, Å	a = 4.0494(3)	a = 4.0309(1)	a = 4.0216(2)	a = 4.006(1)
	c = 10.4987(8)	c = 10.2591(4)	c = 10.1798(5)	c = 10.108(3)
V, Å^3	172.15(2)	166.691(9)	164.64(1)	162.2(1)
Z	2	2	2	2
crystal size, mm^3	0.06 × 0.05 × 0.03	0.07 × 0.05 × 0.05	0.06 × 0.04 × 0.03	0.04 × 0.03 × 0.02
ρ_{calc}, g cm^{-3}	7.788	8.000	7.981	8.070
μ, mm^{-1}	41.267	43.833	43.097	44.325
θ_{max}, deg	37.5	40.0	45.0	36.2
reflections collected	1214	1160	1774	1212
R_{int}	0.021	0.018	0.020	0.021
unique reflections	162	186	239	146
param. refined	11	11	10	10
R_1, wR_2 [$F_0 > 4\sigma(F_0)$]	0.019, 0.045	0.018, 0.041	0.020, 0.052	0.016, 0.037
diff. peak and hole, e Å^{-3}	1.40, −3.07	1.56, −1.74	2.37, −3.87	1.52, −1.61
goodness-of-fit	1.23	1.18	1.59	1.08

[a] Further details of the crystal structure determination may be obtained from Fachinformationszentrum Karlsruhe, D-76344 Eggenstein-Leopoldshafen, Germany, on quoting the depository numbers CSD-422570 (La), 427525 (Ce), 427527 (Pr), and 427528 (Nd). [b] Since the occupancy of the Co site was found to vary slightly from sample to sample, we will use the rounded values for the Co stoichiometry in the following discussion.

temperature range using a home-built phase coherent pulsed NMR/NQR spectrometer. The powder sample was mixed with paraffin and placed in a Teflon sample holder. NMR spectra were recorded by sweeping the magnetic field at several fixed frequencies in the range 24.6−43.2 MHz. The zero-field NMR spectra were measured using a frequency step point-by-point spin−echo technique in the frequency range 13.2−59.8 MHz at 15 K. In all nuclear resonance experiments, the area under the spin echo magnitude was integrated in the time domain and averaged over the scan accumulation number, which depended on the temperature and type of the experiment. Typical pulse lengths were 2−5 μs and 4−10 μs for the π/2- and π-pulses, respectively, with a pulse separation of 15−100 μs, depending on the nucleus, the temperature, and the type of experiment.

Quantum-Chemical Calculations. Density functional band structure calculations using a full potential all-electron local orbital code FPLO (version fplo7.00-28) within the local spin density approximation (LSDA) were performed including spin−orbit coupling.[19] The Perdew−Wang parametrization of the exchange-correlation potentials was employed.[20] Band structures and the density of states (DOS) were calculated after convergence of the total energy on a dense 32 × 32 × 32 mesh with 2393 irreducible k-points. Calculations were performed on two compounds, $LaCo_2As_2$ and $PrCo_2As_2$, using the idealized structures established from single crystal X-ray diffraction, without inclusion of Bi defects or Co vacancies.

The interatomic crystal orbital Hamilton population (COHP) analysis was performed with the tight binding-linear muffin tin orbitals-atomic sphere approximation (TB-LMTO-ASA) software.[21] The von Barth−Hedin exchange−correlation potential was employed for the local density approximation (LDA) calculation.[22] The radial scalar-relativistic Dirac equation was solved to obtain the partial waves. No empty spheres had to be added. The calculations contained a basis set of Pr-6s/5d(6p) with Pr 4f^3 treated as the core, La-6s/5d/4f(6p), Co-4s/4p/3d, P-3s/3p(3d), and As-4s/4p/(4d) (downfolded orbitals in parentheses). A 12 × 12 × 24 mesh with 436 k-points in the irreducible wedge of the tetragonal Brillouin zone was used for integrations over the reciprocal unit cells.[23]

■ RESULTS AND DISCUSSION

Synthesis. In our numerous attempts to repeat the only literature report on the synthesis of RCo_2As_2 in Sn flux,[12] we consistently arrived at samples contaminated by a large amount of byproducts.[13] Thus, we concluded that alternative synthetic conditions were necessary to obtain phase-pure samples. As an alternative, we turned to reactions in molten Bi keeping in mind that this metal does not form any binary compounds with Co and As,[24] and thus, the reaction might proceed in a different pathway as compared to the reaction in Sn flux. Indeed, the reaction between elements in Bi flux led to phase-pure samples of RCo_2As_2 (R = La, Ce, Pr) (Figure 1), although a negligible residual amount of elemental Bi also remains in the sample, as indicated by a very small X-ray diffraction peak at 2θ ~ 28°. When the reactions were scaled up, sufficiently large plate-like single crystals were obtained, with approximate dimensions of 1 × 1 × 0.2 mm^3. The plane of the single crystal is perpendicular to the c axis of the tetragonal structure, as indicated by the strong (00l) peaks in the X-ray powder diffraction pattern collected on a batch of oriented crystals (Supporting Information Figure S1). We could not obtain a phase-pure $NdCo_2As_2$ sample (Supporting Information Figure S2), but a

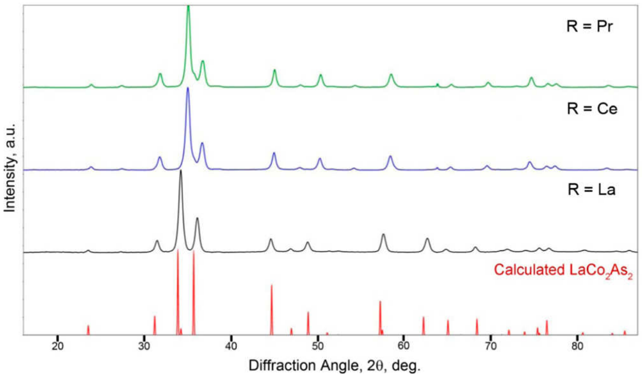

Figure 1. Calculated X-ray powder diffraction pattern of $LaCo_2As_2$ (red) and experimental X-ray powder diffraction patterns of $La_{0.97}Bi_{0.03}Co_{1.9}As_2$ (black), $Ce_{0.95}Bi_{0.05}Co_{1.85}As_2$ (blue), and $PrCo_{1.8}As_2$ (green).

batch of single crystals was manually isolated to characterize the desired product. Attempts to prepare the analogous Sm- or Gd-containing compounds were unsuccessful, although the isostructural phosphide, $SmCo_2P_2$, is known.[8b]

Crystal Structure. Single-crystal X-ray diffraction confirmed that all RCo_2As_2 phases crystallize in the $ThCr_2Si_2$ structure type, space group *I*4/*mmm* (Figure 2). The EDX analysis revealed the average elemental ratio R/Co/As ~ 1.2:1.8:2 (Table 2), which is close to the nominal 1:2:2 stoichiometry. The refinement of the crystal structure indicated the formation of ~5−15% vacancies in the Co sublattice, which is in agreement with the slightly lower Co content detected by the EDX analysis. In addition, both La- and Ce-containing crystals showed significant residual electron density nearby the rare-earth crystallographic site (Wyckoff position 2*a*). The electron density peak was positioned at ~0.5 Å away from the rare-earth site and could not be accounted for by the anisotropic atomic displacement of the R atom. Therefore, this site was assigned as partially occupied by Bi atoms, and the total occupancy of the R and Bi sites was constrained to 1. The incorporation of the extra atomic site into the structure of $LaCo_2As_2$ obtained from Bi flux is supported by the substantial increase of the unit cell parameter *c* for this material as compared to the sample of $LaCo_2As_2$ prepared in the absence of Bi flux[12] (Table 2). It is puzzling, however, that the structure of $CeCo_2As_2$, which also reveals such dopant site, has nearly the same *c* parameter when prepared with or without Bi flux. The *c* parameter also remains nearly the same for both samples of $PrCo_2As_2$ or $NdCo_2As_2$, and no evidence for the Bi doping was observed in the structure of these compounds. The crystal structure refinement led to the final compositions $La_{0.97}Bi_{0.03}Co_{1.9}As_2$, $Ce_{0.95}Bi_{0.05}Co_{1.85}As_2$, $PrCo_{1.8}As_2$, and $NdCo_{1.7}As_2$. Noteworthy, a similar inclusion of Sn into the structure of $BaFe_2As_2$ was observed for the synthesis of this compound in Sn flux,[25] while the formation of vacancies in the transition-metal sites was also found for other $ThCr_2Si_2$-type arsenides, for example, $BaAg_{1.93}As_2$, $BaCu_{1.88}As_2$, and $CeNi_{1.76}As_2$.[26] We also note that the presence of a small amount (<2%) of Bi was conclusively established from the EDX microanalysis, but the accuracy of the determination is not sufficient to make a quantitative judgment about the Bi content against other elements present in the sample.

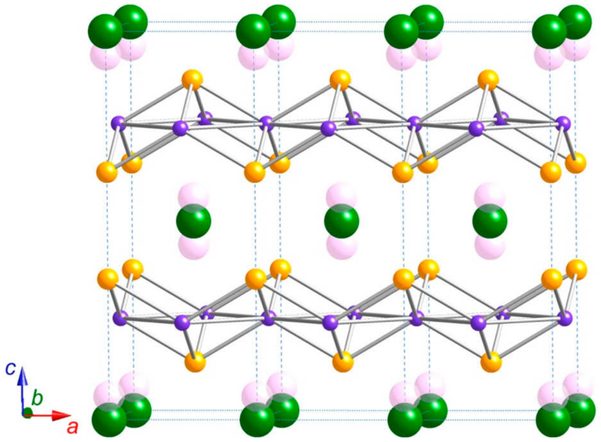

Figure 2. Crystal structure of $La_{0.97}Bi_{0.03}Co_{1.9}As_2$ showing three adjacent unit cells along the *a* axis. Color scheme: La = green, Co = purple, As = orange. The Bi sites are shown with translucent pink to emphasize the low partial occupancy of these positions.

In the crystal structures of $La_{0.97}Bi_{0.03}Co_{1.9}As_2$ and $Ce_{0.95}Bi_{0.05}Co_{1.85}As_2$, the displacement of the Bi site relative to the more symmetric R site can be explained by the necessity to accommodate the stereoactive 6s^2 lone pair of the Bi^{3+} ion. This displacement results in a distorted coordination environment around Bi, with four longer and four shorter Bi−As bonds, as compared to the unique length of the eight R−As bonds (Table 3). The Bi inclusion, however, is not observed in the Pr- and Nd-containing structures, despite the presence of Co vacancies. This difference can be tentatively explained by the lanthanide contraction, which makes the lanthanide coordination cage less accommodating to the Bi^{3+} ion (cf. ionic radii: Bi^{3+}, 1.17 Å; La^{3+}, 1.16 Å; Ce^{3+}, 1.14 Å; Pr^{3+}, 1.13 Å; Nd^{3+}, 1.11 Å). The substitution of Bi for lanthanides is not unprecedented; for example, it is well established for rare-earth ferrite garnets.[27]

It is also noteworthy that the interlayer As−As distance in RCo_2As_2 changes quite consistently with the ionic radius of the R^{3+} ions, from 2.880(2) Å for R = La to 2.7215(6) Å for R = Nd (Table 3), in contrast to RCo_2P_2, where the interlayer P−P separation for R = La (3.162 Å) greatly exceeds the P−P distances for the other members of the series (~2.5−2.6 Å).[8b] Another structural difference can be gleaned from the

Table 2. Results of EDX Analysis and Crystallographic Parameters of $R_{1-x}Bi_xCo_{2-\delta}As_2$ Determined by Room-Temperature Powder X-ray Diffraction[a]

phase	EDX anal.	*a*, Å	*c*, Å	*V*, Å^3
$LaCo_2As_2$[12]		4.054	10.328	169.8
$La_{0.97}Bi_{0.03}Co_{1.9}As_2$[b]	1.20(1):1.79(1):2	4.0508(2)	10.470(1)	171.80(1)
$LaCo_2P_2$[8b]		3.815	11.041	160.6
$CeCo_2As_2$[12]		4.026	10.216	165.6
$Ce_{0.95}Bi_{0.05}Co_{1.85}As_2$[b]	1.19(3):1.76(4):2	4.0284(8)	10.217(2)	165.81(1)
$CeCo_2P_2$[8b]		3.894	9.599	145.5
$PrCo_2As_2$[12]		4.017	10.169	164.1
$PrCo_{1.8}As_2$[b]	1.19(9):1.8(1):2	4.0211(5)	10.167(1)	164.40(1)
$PrCo_2P_2$[8b]		3.900	9.759	148.4
$NdCo_2As_2$[12]		4.006	10.078	161.7
$NdCo_{1.7}As_2$[b]	1.15(5):1.61(4):2	4.014(4)	10.09(1)	162.53(2)
$NdCo_2P_2$[8b]		3.891	9.687	146.7

[a] A comparison to the parameters of RCo_2P_2 is also provided. [b] The R/Co/As atomic ratio. The amount of Bi in the La- and Ce- containing samples could not be established from the EDX analysis due to the low content of this element.

Table 3. Interatomic Distances (Å) in the $R_{1-x}Bi_xCo_{2-\delta}As_2$ Structures As Determined by Single-Crystal X-ray Diffraction Analysis at 298 K

compd.	R–As	Bi–As	R–Co	Bi–Co	As–As	Co–Co
$La_{0.97}Bi_{0.03}Co_{1.9}As_2$	3.2068(3)	3.12(2) 3.31(2)	3.3149(2)	3.15(3) 3.49(2)	2.8880(2)	2.8634(2)
$Ce_{0.95}Bi_{0.05}Co_{1.85}As_2$	3.1675(3)	3.09(1) 3.26(1)	3.2619(1)	3.18(2) 3.34(3)	2.7634(4)	2.8503(4)
$PrCo_{1.8}As_2$	3.1556(2)		3.2435(1)		2.7361(1)	2.8437(1)
$NdCo_{1.7}As_2$	3.1427(8)		3.2247(7)		2.7215(6)	2.8329(8)

comparison of the Co–Co distances. In RCo_2P_2, the decrease in the interlayer P–P distance resulted in a significant increase in the intralayer Co–Co distance,[9] but in RCo_2As_2 both As–As and Co–Co distances decrease with the lanthanide contraction (Table 3). Similar to the shorter P–P distances in RCo_2P_2, the As–As distances in RCo_2As_2 notably exceed the typical length of the As–As single bond (2.43 Å),[28] suggesting the absence of any significant As–As bonding in these structures. Thus, the interlayer cohesion between the $[Co_2As_2]$ slabs is mainly provided by the R–As bonding.

XANES Spectroscopy. Based on the analysis of magnetic properties and unit cell volumes of the RCo_2P_2 series, Jeitschko et al. deduced that Ce atoms exhibit valence fluctuations in $CeCo_2P_2$.[8b] These earlier findings incited us to examine the oxidation state of Ce in $Ce_{0.95}Bi_{0.05}Co_{1.85}As_2$ by means of XANES spectroscopy at the L_3 edge of Ce. A spectrum obtained at room temperature is shown in Figure 3. It can be deconvoluted into two contributions corresponding to Ce^{3+} and Ce^{4+} oxidation states. The former component clearly dominates the spectrum. Therefore, $Ce_{0.95}Bi_{0.05}Co_{1.85}As_2$ can be classified as a slightly mixed-valent compound with the average oxidation state of Ce equal to +3.06, which remains essentially the same from 10 to 300 K (Supporting Information Figure S3, Table S1). The XANES measurements also confirmed that the oxidation states of La in $La_{0.97}Bi_{0.03}Co_{1.9}As_2$ and Pr in $PrCo_{1.8}As_2$ are equal to +3 (Supporting Information Figure S4).

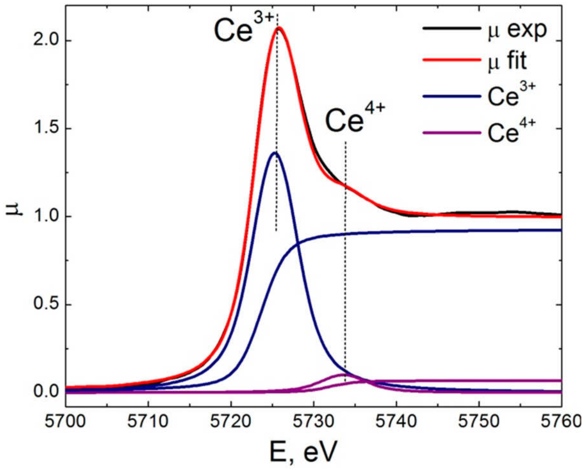

Figure 3. L_3-Ce XANES spectrum of $Ce_{0.95}Bi_{0.05}Co_{1.85}As_2$ at room temperature.

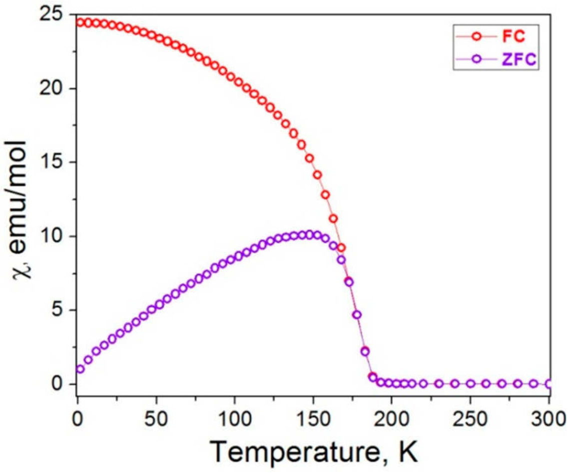

Figure 4. Temperature dependence of zero-field-cooled (ZFC) and field-cooled (FC) magnetic susceptibilities of a polycrystalline sample of $La_{0.97}Bi_{0.03}Co_{1.9}As_2$ measured under magnetic field of 1 mT.

Magnetic Properties. *$La_{0.97}Bi_{0.03}Co_{1.9}As_2$.* Magnetic measurements on a polycrystalline sample of $La_{0.97}Bi_{0.03}Co_{1.9}As_2$ revealed that this compound exhibits FM ordering at T_C = 178 K (Figure 4), where the T_C value was determined from the minimum of the $d\chi/dT$ derivative curve. A negligible coercivity observed in the hysteresis loop measured at 1.8 K indicates that $La_{0.97}Bi_{0.03}Co_{1.9}As_2$ is a soft ferromagnet (Supporting Information Figure S5). Nevertheless, the divergence of the zero-field-cooled (ZFC) and field-cooled (FC) susceptibility curves suggests some magnetic anisotropy in the Co sublattice.

To further investigate the magnetic anisotropy of $La_{0.97}Bi_{0.03}Co_{1.9}As_2$, magnetic measurements were performed on an oriented single crystal of this compound. The magnetic field (H = 1 mT) was applied parallel and perpendicular to the tetragonal c axis, revealing a strong preference of the Co moments to be magnetized along the c axis (Figure 5a). With $H \| c$, the magnetization is saturated already at ~0.1 T, while with $H \perp c$, the saturation is reached only at ~6.5 T (Figure 5b). Based on the field-dependent magnetization data collected at 1.8 K, the saturation magnetization value is 0.59(1) μ_B per Co atom. Interestingly, the preferred alignment of Co moments in $La_{0.97}Bi_{0.03}Co_{1.9}As_2$ differs dramatically from that found in the magnetic structure of $LaCo_2P_2$, where the Co moments exhibit FM alignment parallel to the ab plane.[29]

$Ce_{0.95}Bi_{0.05}Co_{1.85}As_2$. Magnetic measurements on a polycrystalline sample of $Ce_{0.95}Bi_{0.05}Co_{1.85}As_2$ reveal FM ordering at T_C = 147 K (Figure 6a). By comparison to the La-containing analogue, this phase transition can be attributed to the ordering of Co magnetic moments. The divergence of the ZFC and FC susceptibility curves also indicates the presence of magnetic anisotropy. The ZFC-FC data, however, do not reveal directly the contribution of Ce to the magnetism of this material, although one should expect such contribution to be significant, given that the Ce ions in this compound are mainly in the +3 oxidation state (Figure 3). The isothermal field dependence of magnetization collected at different temperatures (Figure 6b)

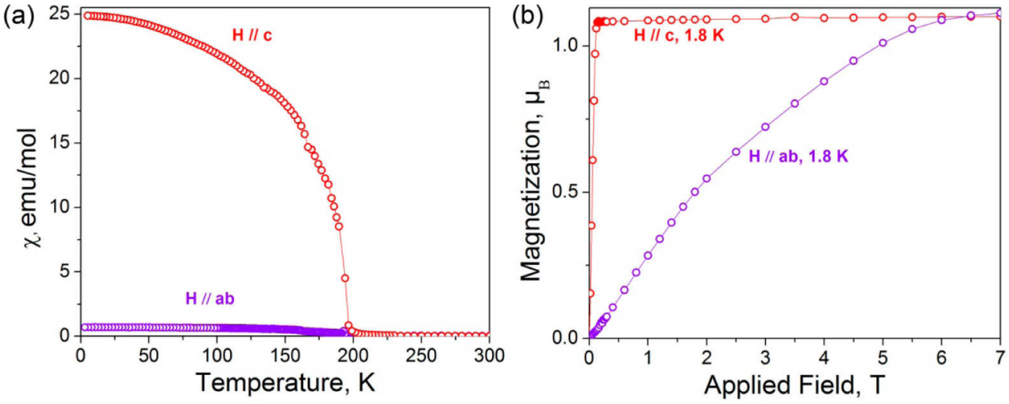

Figure 5. Temperature dependence of magnetic susceptibility at 1 mT (a) and field dependence of magnetization at 1.8 K (b) measured on a single crystal of $La_{0.97}Bi_{0.03}Co_{1.9}As_2$ with the magnetic field applied parallel or perpendicular to the *c* axis.

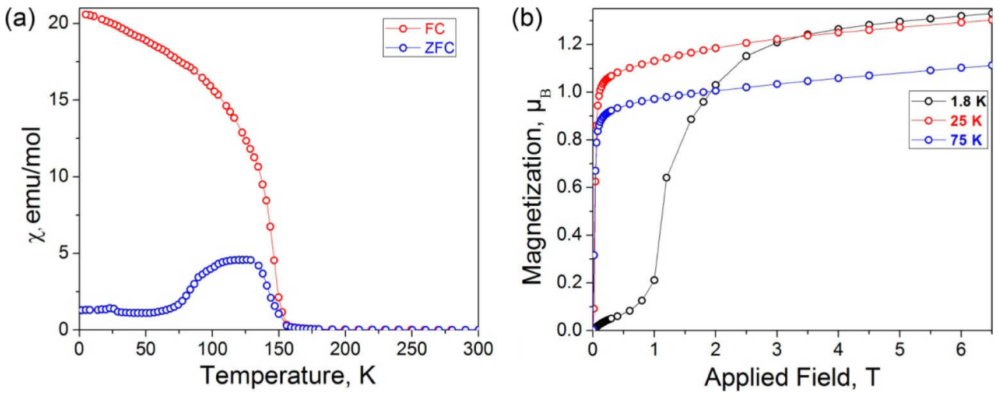

Figure 6. Magnetic measurements on a polycrystalline sample of $Ce_{0.95}Bi_{0.05}Co_{1.85}As_2$: (a) Temperature dependence of zero-field-cooled (ZFC) and field-cooled (FC) magnetic susceptibilities measured under applied field of 1 mT. (b) Isothermal field dependence of magnetization at 1.8, 25, and 75 K.

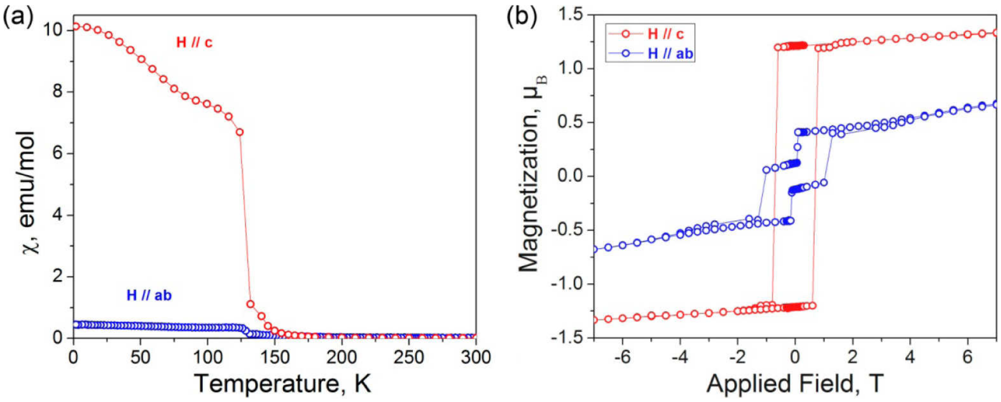

Figure 7. Magnetic measurements on an oriented single crystal of $Ce_{0.95}Bi_{0.05}Co_{1.85}As_2$: Temperature dependences of FC magnetic susceptibilities at 1 mT (a) and hysteresis loops at 1.8 K (b) measured with the magnetic field applied parallel and perpendicular to the *c* axis.

exhibits fast increase in magnetization at 75 K due to the ordered Co moments followed by the gradual linear increase due to the paramagnetic disordered Ce moments. The magnetization curve obtained at 25 K is nearly the same, with the slightly larger initial increase, as can be expected from the better alignment of the FM ordered Co domains due to the lower thermal energy. The field-dependent magnetization collected at 1.8 K, however, shows a substantial coercivity that must be emerging from the ordering of Ce magnetic moments with high magnetocrystalline anisotropy.

The magnetic anisotropy of Co and Ce sublattices can be observed in the single-crystal magnetic measurements. Similar to $La_{0.97}Bi_{0.03}Co_{1.9}As_2$, the magnetic moments show a strong preference to ordering along the *c* axis (Figure 7a). Besides the sharp rise below T_C = 147 K due to the ordering of 3*d* moments, another feature is observed in the susceptibility curve around 70 K. This anomaly is probably associated with the gradual ordering of 4*f* moments. The hysteresis loop measured at 1.8 K with $H \| c$ (Figure 7b) exhibits large coercivity (0.6 T) and remanence (1.2 μ_B) associated with the high magnetocrystalline anisotropy of the Ce sublattice. With $H \perp c$, the coercivity becomes even larger (1 T) but the saturation magnetization is substantially lower and the remnant magnetization drops nearly to zero when the magnetic field is removed.

At this point, we need to consider the possible nature of magnetic exchange between the 3*d* moments of Co and the 4*f* moments of Ce. In the case of related RCo_2 intermetallics, it was established that the 3*d*-4*f* exchange is always FM for the lighter rare-earth ions, with less than half-filled 4*f* subshell. The theoretically expected magnetization of the Ce^{3+} ion is equal to 2.14 μ_B, or, when corrected for the oxidation state of Ce (+3.06) found from XANES spectra, 2.01 μ_B in $Ce_{0.95}Bi_{0.05}Co_{1.85}As_2$. The magnetic moment per Co atom can be approximated as 0.59 μ_B from the magnetic properties of $La_{0.97}Bi_{0.03}Co_{1.9}As_2$ (Figure 5b), which is also close to the value found from the initial increase in the magnetization of $Ce_{0.95}Bi_{0.05}Co_{1.85}As_2$ at 25 K (Figure 6b). Hence, if the Ce and Co moments were parallel to each other, the total expected saturation magnetization would be equal to ~3.09 μ_B, taking into account the composition of the compound. This is much higher than the actual saturation value of 1.33 μ_B observed at 1.8 K. On the other hand, if we assume AFM 3*d*-4*f* exchange, the expected saturation magnetization should be ~0.73 μ_B, which is closer to the value observed, but still somewhat lower. This analysis of magnetization data suggests noncollinear AFM coupling between the Ce and Co magnetic moments in $Ce_{0.95}Bi_{0.05}Co_{1.85}As_2$. This hypothesis is also in agreement with our recent finding of FiM ordering in $La_{0.75}Pr_{0.25}Co_2P_2$.[10] We also note that the magnetic behavior of $Ce_{0.95}Bi_{0.05}Co_{1.85}As_2$ is strikingly different from that of $CeCo_2P_2$, which exhibits AFM ordering in both Ce and Co sublattices.[30] Later, in the neutron diffraction section, we will return to the discussion of the magnetic ordering in $Ce_{0.95}Bi_{0.05}Co_{1.85}As_2$.

$PrCo_{1.8}As_2$. Similar to the La- and Ce- containing analogues, $PrCo_{1.8}As_2$ exhibits FM ordering of Co moments at T_C = 140 K, as shown by the ZFC and FC susceptibility measurements on a polycrystalline sample (Figure 8). This behavior is strikingly different from the isostructural phosphide, $PrCo_2P_2$, where the Co moments show AFM ordering at T_N = 309 K.[9] In the low-temperature range, a significant decrease in the magnetic moment is observed below 50 K. Such magnetic behavior of $PrCo_{1.8}As_2$ is similar to the behavior of $La_{0.75}Pr_{0.25}Co_2P_2$,[10] suggesting AFM coupling between the 3*d* and 4*f* magnetic moments. The temperature-dependent FC susceptibility curve is typical of a ferrimagnet with different anisotropies of two magnetic sublattices.[31] As the temperature is decreased below T_C, the soft Co moments order first, causing the abrupt increase in the magnetization, while the hard Pr moments order gradually under the influence of the internal magnetic field induced by the Co moments, resulting in the decrease in the total magnetization value. At T_{comp} = 9 K, the contributions from both sublattices become nearly equal, which leads to the observation of zero magnetization at this temperature and negative magnetization values below 9 K, a phenomenon known as the magnetic pole reversal.[31a]

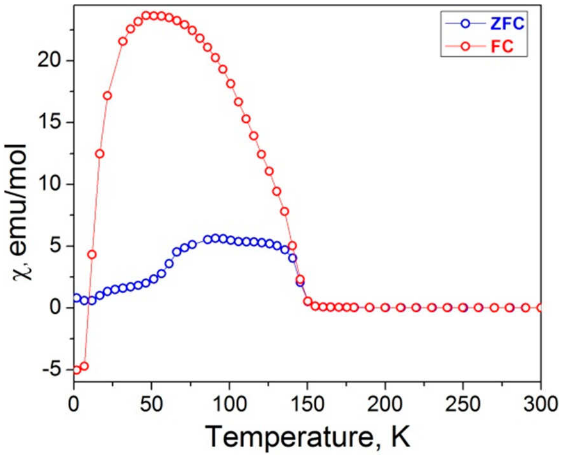

Figure 8. Temperature dependence of zero-field-cooled (ZFC) and field-cooled (FC) magnetic susceptibilities of a polycrystalline sample of $PrCo_{1.8}As_2$ measured under magnetic field of 1 mT.

The anisotropy of magnetic properties is observed in the magnetic measurement on a single crystal of $PrCo_{1.8}As_2$. Similar to $La_{0.97}Bi_{0.03}Co_{1.9}As_2$ and $Ce_{0.95}Bi_{0.05}Co_{1.85}As_2$, the magnetic moments prefer to order along the *c* axis (Figure 9a). The field-dependent magnetization measured with $H\|c$ at 100 K exhibits an abrupt increase, confirming the FM ordering in the magnetically soft Co sublattice (Figure 9b), while with $H\perp c$ the magnetization increases slowly, as expected for the direction perpendicular to the easy axis (Supporting Information Figure S6a). A gradual linear increase in the $H\|c$ magnetization is observed as the field increases, which confirms the paramagnetism of the Pr sublattice at 100 K. At 30 K, this linear increase becomes much more pronounced, in agreement with the purported gradual ordering of the Pr moments under the influence of the FM ordered Co sublattice. The magnetic moment per Co atom estimated from the initial ordering of Co moments at 30 K equals to 0.37 μ_B. The magnetization behavior at 1.8 K is very different. Instead of the fast initial rise, we observe a gradual linear increase to a plateau of 1.4 μ_B followed by a metamagnetic transition at H_{cr} = 4.2 T and saturation of the total magnetization at 3.0 μ_B. This value is slightly lower than the theoretical expectation for the Pr^{3+} ion (3.2 μ_B) and thus suggests a noncollinear AFM coupling between the Pr and Co moments, similar to the situation observed in $Ce_{0.95}Bi_{0.05}Co_{1.85}As_2$. The magnetization behavior measured on a polycrystalline sample of $PrCo_{1.8}As_2$ at 1.8 and 100 K (Supporting Information Figure S6b) is very similar to that observed for the single-crystal sample with $H\|c$.

It appears, however, that the noncollinear FiM state in $PrCo_{1.8}As_2$ is only stabilized at high fields, because the metamagnetic behavior at lower fields suggests the initial presence of an AFM state. We also note a small feature around 7 K in the temperature-dependent FC magnetization curve at $H\|c$ (Figure 9a), which indicates a possible second (AFM) magnetic phase transition in $PrCo_{1.8}As_2$. Indeed, an examination of a hysteresis curve recorded for the single crystal of $PrCo_{1.8}As_2$ at 1.8 K (Figure 10) reveals two metamagnetic transitions, with the critical fields of 1.3 and 4.4 T. As the field is increased in either positive or negative direction, the initial small increase of magnetization to ~0.5 μ_B is followed by the first metamagnetic step to 1.3 μ_B and then by the second metamagnetic step to 2.9 μ_B. Taking into account the possible magnitudes of the Co 3*d* and Pr 4*f* magnetic moments discussed above, the stepwise growth of magnetization appears to correspond to the FM magnetization of Co moments, followed by switching of a half of Pr moments from the AFM to FM order at ~1.5 T, and finally by switching of the other half of Pr moments from the AFM to FM order at ~4.5 T. In both metamagnetic transitions, the reoriented Pr 4*f* moments become coupled AFM to the Co 3*d* moments. Such sequence

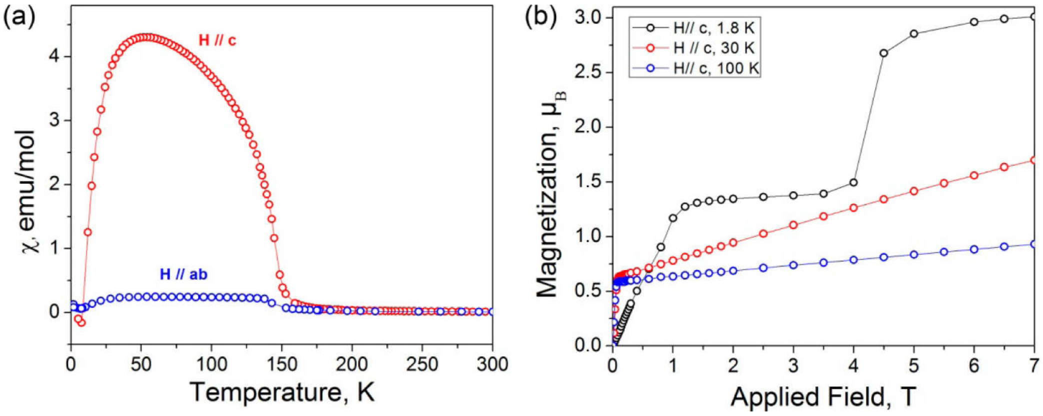

Figure 9. Magnetic measurements on an oriented single crystal of $PrCo_{1.8}As_2$. (a) Temperature dependences of FC magnetic susceptibilities with the field of 1 mT applied parallel and perpendicular to the *c* axis. (b) Isothermal field dependences of magnetization at 1.8, 30, and 100 K with the field applied parallel to the *c* axis.

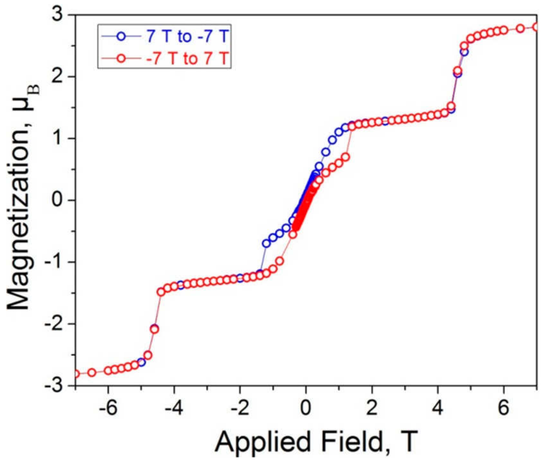

Figure 10. Hysteresis loop for a single crystal of $PrCo_{1.8}As_2$ recorded at 1.8 K with magnetic field applied parallel to the *c* axis. The blue and red portions of the curves were collected upon changing the field from 7 to −7 T and from −7 to 7 T, respectively.

of field-dependent magnetic phase transitions is also in agreement with the larger increase in the total moment at the second step as compared to the increase at the first step. Nevertheless, it is not clear why the Pr moment should reorient in such a stepwise manner. At the very least, these observations suggest the structure of the magnetically ordered ground state might be more complicated than just simple alignment of moments parallel to the *c* axis. Further studies, including neutron diffraction, X-ray magnetic circular dichroism spectroscopy, and magnetoresistance measurements, will be undertaken to verify the proposed scenario and establish the field-dependent magnetic structures.

$NdCo_{1.7}As_2$. We were not able to obtain a phase-pure sample of $NdCo_{1.7}As_2$, and the crystals of this compound were too small for single-crystal magnetic measurements. Therefore, the measurements were performed only on a batch of several manually selected crystals. The magnetic behavior of $NdCo_{1.7}As_2$ is similar to that of $PrCo_{1.8}As_2$. The FM ordering of Co moments at T_C = 62 K is followed by an abrupt decrease in the FC susceptibility nearly to zero at lower temperatures (Figure 11a), in agreement with AFM 3*d*-4*f* exchange. Another turning point in the χ vs T curve is observed at 6 K. The field-dependent magnetization at 1.8 K also reveals two metamagnetic transitions (Figure 11b). The first critical field is ∼3.5 T while only an onset of the second field-induced event is observed at 7 T, with the maximum saturation value of 1.66 μ_B reached at this field. Since the expected saturation magnetization per Nd^{3+} ion is 3.28 μ_B, it appears that, similar to $PrCo_{1.8}As_2$, the two metamagnetic transitions correspond to the stepwise reorientation of the Nd magnetic moments to afford the FiM ground state.

Neutron Powder Diffraction. Jeitschko et al. established the magnetic structures of the isostructural compounds RCo_2P_2

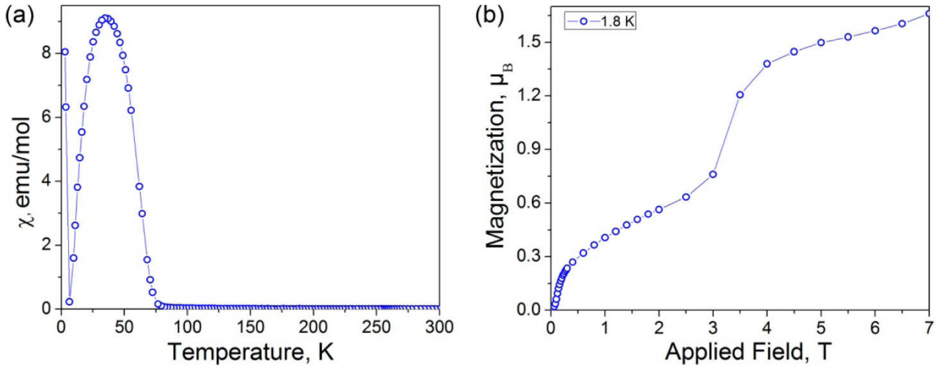

Figure 11. Magnetic measurements on a polycrystalline sample of $NdCo_{1.7}As_2$. (a) Temperature dependence of field-cooled magnetic susceptibilities measured under applied magnetic field of 10 mT. (b) Isothermal field dependence of magnetization at 1.8 K.

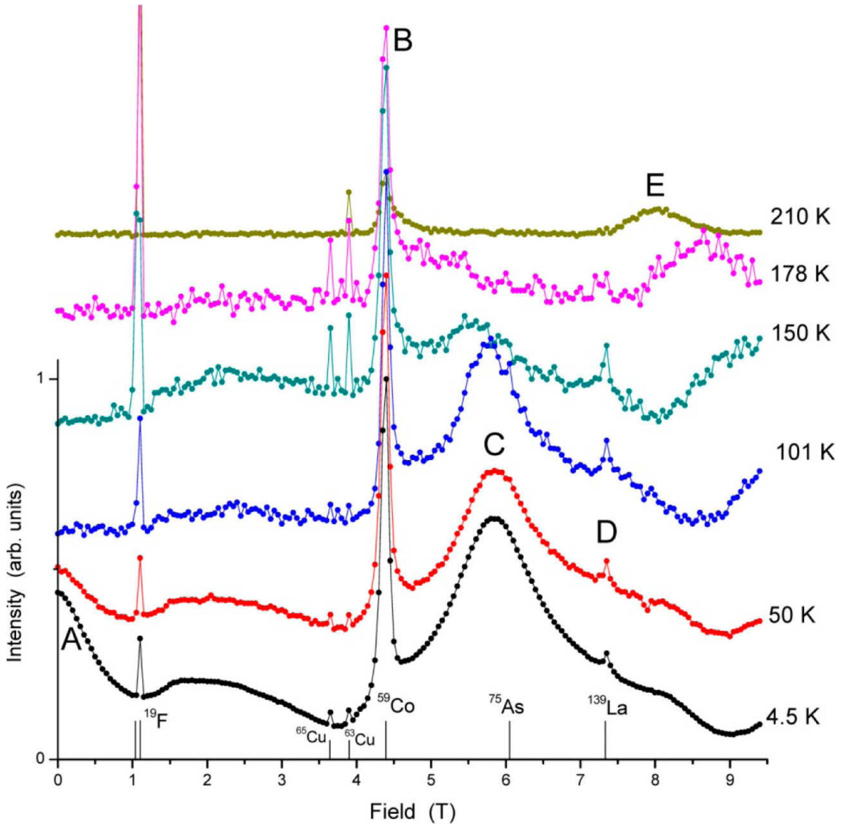

Figure 12. NMR spectra of $La_{0.97}Bi_{0.03}Co_{1.9}As_2$ measured at 44.1 MHz for different temperatures. The positions of the free Larmor precessions of all nuclei under investigation are shown by short vertical lines. Extrinsic signals ^{1}H, ^{19}F, and ^{65,63}Cu are due to the experimental set-up.

by neutron diffraction studies.[29,30,32] We also turned to this method to probe the magnetic structures of $La_{0.97}Bi_{0.03}Co_{1.9}As_2$ and $Ce_{0.95}Bi_{0.05}Co_{1.85}As_2$. (We could not perform such studies on $PrCo_{1.8}As_2$ because attempts to scale up the preparation did not afford sufficiently pure samples.) The diffraction data were collected above and below the magnetic ordering temperatures but did not reveal any magnetic peaks below T_C. Rietveld refinement of the nuclear structure of both compounds resulted in the unit cell parameters $a = 4.0592(1)$ Å, $c = 10.4830(5)$ Å for R = La and $a = 4.0396(2)$ Å, $c = 10.2202(5)$ Å for R = Ce, in good agreement with the values refined from the room-temperature powder X-ray diffraction data (Table 2). The structural refinements led to formulas $LaCo_{1.73}As_2$ and $CeCo_{1.8}As_2$, respectively (Supporting Information Figures S7 and S8, Table S2), which confirm the presence of Co vacancies established from the single-crystal X-ray diffraction data. The occupancy of the possible Bi site was not refined, due to the very similar scattering lengths of Bi (8.532 fm) and La (8.24 fm) and the low amount of Bi present in the structures. Nevertheless, we note yet again the significantly larger c parameter of the La-containing samples obtained from Bi flux (10.470(1) Å from X-ray and 10.4830(5) Å from neutron powder diffraction) as compared to the c parameter reported for the sample obtained by a solid-state reaction between the elements (10.328 Å).[12]

One shall note that the FM ordering of Co moments along the c axis is expected to produce magnetic scattering at the (110) reflection, which contains a significant nuclear scattering contribution. This is in contrast to the neutron diffraction patterns of FM $LaCo_2P_2$[29] and $La_{0.75}Pr_{0.25}Co_2P_2$[10] where the presence of a weak magnetic (002) reflection is caused by the FM ordering of Co moments in the ab plane. The relatively large structure factor associated with the nuclear component of the (110) reflection in RCo_2As_2 (Supporting Information Figure S9) introduces a strong limitation on the magnitude of the FM moment that can be detected by using unpolarized neutrons. Indeed, our simulation of the neutron powder diffraction patterns of $LaCo_{1.73}As_2$ and $CeCo_{1.8}As_2$ for the experimentally determined FM ordering of 3d moments along the c axis (~0.6 μ_B per Co atom) demonstrates that the contribution of this magnetic structure to the pattern is negligible (Supporting Information Figure S10). On the other hand, if one assumed antiparallel alignment of 3d and 4f moments at lower temperatures, with the calculated moment of ~2.0 μ_B per Ce atom, both (110) and (101) reflections should have been strongly enhanced, but we do not observe such enhancement experimentally. Neither can we reject magnetic ordering in the Ce sublattice, given the large magnetic hysteresis found for $Ce_{0.95}Bi_{0.05}Co_{1.85}As_2$ in contrast to the magnetic softness of $La_{0.97}Bi_{0.03}Co_{1.9}As_2$. All these considerations lead us to believe that the lowest-temperature magnetic structure of $Ce_{0.95}Bi_{0.05}Co_{1.85}As_2$ involves, at the very least, noncollinear AFM arrangement between the Ce and Co moments, if not an even more complicated magnetic ordering. Polarized neutron diffraction experiments able to provide increased sensitivity to the FM ordering along the c axis in both R and Co sublattices are planned for the future.

Solid-State NMR Spectroscopy. NMR spectroscopy experiments were carried out on a polycrystalline sample of $La_{0.97}Bi_{0.03}Co_{1.9}As_2$. There are three NMR active nuclei in this material: ^{59}Co, ^{75}As, and ^{139}La. In addition to these intrinsic isotopes, we observed extrinsic NMR signals which were

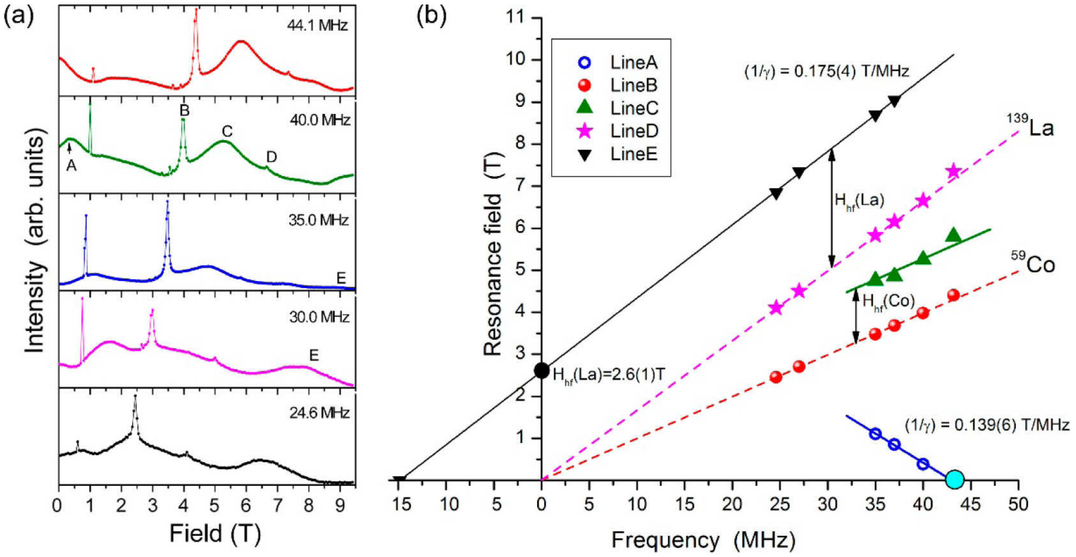

Figure 13. (a) NMR spectra of $La_{0.97}Bi_{0.03}Co_{1.9}As_2$ measured at different frequencies at 4.7 K. (b) Frequency dependence of the resonance field H for lines A–E shown in the spectra of the panel (a). Linear relations $H(\nu) = (\gamma/2\pi)^{-1}\nu$ due to the free Larmor precession are plotted for the ^{59}Co (solid green and dashed red lines), ^{139}La (solid black and dashed magenta lines), and ^{75}As (solid blue line) nuclei. The linear fits for the intrinsic signals of the $La_{0.97}Bi_{0.03}Co_{1.9}As_2$ phase and for the signals of impurity phases are shown with solid and dashed lines, respectively.

introduced due to the experimental set up, that is, ^{1}H from paraffin, ^{19}F from the Teflon sample holder, and ^{63,65}Cu from the copper coil of the tank circuit. Field-sweep NMR spectra measured at a fixed frequency of 44.1 MHz for different temperatures are shown in Figure 12. As the temperature is lowered, the spectra become more complex, and the one at 4.5 K demonstrates a complicated shape with several broad lines in the entire magnetic field range available (0–9.4 T). In order to assign these lines properly, we measured isothermal field-sweep NMR spectra at 4.7 K at various fixed frequencies (Figure 13a). The field positions of characteristic resonance lines are labeled A–E in Figures 12 and 13a and are plotted as a function of frequency in Figure 13b, following the approach developed by us earlier.[33] In this figure, we also plot solid lines that give the linear relation $H(\nu) = (\gamma/2\pi)^{-1}\nu$, according to the free Larmor precessions of the ^{59}Co ($\gamma/2\pi$ = 10.05 MHz/T), ^{75}As ($\gamma/2\pi$ = 7.29 MHz/T), and ^{139}La ($\gamma/2\pi$ = 5.62 MHz/T) nuclei.

An analysis of the frequency dependence of resonance fields reveals that lines B and D belong to minor impurity phases. Thus, one can easily assign the intensive and narrow line B to ^{59}Co nuclei in the diamagnetic cubic impurity phase (exactly observed at the position of the free Larmor precession, $\gamma/2\pi$ = 10.05 MHz/T, without any shift or quadrupole splitting). The very small line D originates from ^{139}La nuclei of some La-containing impurity. The corresponding linear dependences are shown in Figure 13b with dashed red (B, ^{59}Co) and magenta (D, ^{139}La) lines. The minor impurity might be the cubic $LaCoO_3$ phase, but its amount was below the detection limit of powder X-ray diffraction.

The other three lines, A, C, and E, can be assigned to the major phase, $La_{0.97}Bi_{0.03}Co_{1.9}As_2$, as their positions and intensities change significantly as the temperature is increased above the Curie point, T_C = 178 K. Thus, the high-field line E shifts to lower fields, toward the ^{139}La Larmor field value, with increasing temperatures above 150 K (cf. Figure 12). The best fit of the H vs ν data for this signal is shown with the solid black line (Figure 13b), which gives the linear coefficient of 0.175(4) T/MHz, close to $(^{139}\gamma/2\pi)^{-1}$ = 0.166 T/MHz. From the intercept of this linear fit with the resonance field axis (black circle) one obtains the value of the hyperfine field at the La site in $La_{0.97}Bi_{0.03}Co_{1.9}As_2$ to be $H_{hf}(La)$ = 2.6(1) T.

The broad line C also shifts to lower fields, toward the ^{59}Co Larmor field value, with increasing temperature and merges with the ^{59}Co line B from the impurity phase for $T > 170$ K (Figure 12), resulting in the solitary, asymmetric line observed at the ^{59}Co Larmor field for 210 K. Such temperature behavior of the chemical shift unambiguously proves that the line C originates from ^{59}Co nuclei. Therefore, the H vs ν data for this signal were fitted to the linear function, $H = a\nu + b$ (solid green line in Figure 13b), with the coefficient $a = (^{59}\gamma/2\pi)^{-1} = 0.0995$ T/MHz. The best-fit constant term b gives the value of the hyperfine field at the Co site in $La_{0.97}Bi_{0.03}Co_{1.9}As_2$ to be $b = H_{hf}(Co) = 1.3(1)$ T. This value of the hyperfine field H_{hf} is very small, in comparison to that at the La site. Probably, this line represents not all Co atoms but only those nearest to the Bi defects at the La sites, where the hyperfine field is strongly reduced due to the high diamagnetism of the Bi atoms. This assumption is strongly corroborated by the fact that our ^{59}Co spectral lines in $La_{0.97}Bi_{0.03}Co_{1.9}As_2$ exhibit *no* splitting in central and satellite contributions due to the interaction of the nuclear electric quadruple moment with the surrounding electrical field gradient (EFG). In general, the $ThCr_2Si_2$-type structures exhibit an appreciable EFG with axial symmetry along the crystallographic c-axis at the transition metal site,[34] but a distortion of the local EFG due to Bi defects at the La sites yields a collapse of the spectral pattern with distinct central and satellite contributions into one, solitary broad single line, as we observe for the Co site.

To validate this assignment and for better understanding of the low-temperature magnetic structure of $La_{0.97}Bi_{0.03}Co_{1.9}As_2$, we performed zero-field NMR measurements at 15 K sweeping the irradiation frequency, ν, step-by-step. Although the spectrum is rather broad and complicated, it contains two distinct lines (Figure 14). The left narrow peak corresponds to the ^{139}La zero-field NMR signal originating from the non-disturbed by Bi defects La sites with nearly zero electric field

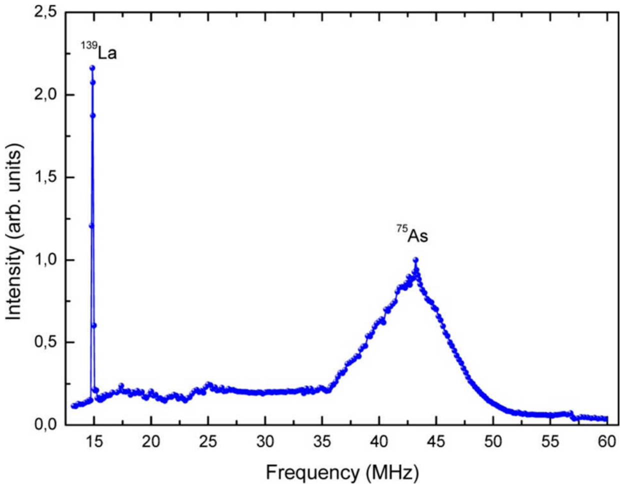

Figure 14. Zero-field NMR spectrum of $La_{0.97}Bi_{0.03}Co_{1.9}As_2$ measured at 15 K.

gradient (EFG). Taking into account the Larmor precession of the ^{139}La nucleus ($\gamma/2\pi$ = 5.62 MHz/T), the position of this peak provides an estimate of the local field at the La site to be 2.59(2) T. This value is in a very good agreement with the value of the hyperfine field H_{hf}(La) estimated from the line E in the H vs ν diagram (shown as black circle in Figure 13b).

Finally, the position of the broad NMR peak at ~43.2 MHz (Figure 14) coincides well with the low-field line A in the H vs ν diagram (Figure 13b, cyan circle). This line shows an opposite frequency dependence with the absolute value of the linear coefficient equal to 0.139(6) T/MHz, which is in perfect agreement with the value of inverse Larmor precession expected for ^{75}As: $(^{75}\gamma/2\pi)^{-1}$ = 0.137 T/MHz. From the peak frequency of 43.2(1) MHz one estimates the value of the hyperfine field to be H_{hf}(As) = 5.92 T.

Actually, in the zero-field NMR spectrum the spin−echo intensity was observed in the entire frequency range 13−65 MHz (Figure 14). This might be due to the wide distribution of local magnetic fields and EFGs on the Co and As sites in the vicinity of Bi defects. Overall, we observed very complicated field-sweep NMR spectra and the broad zero-field NMR spectrum for $La_{0.97}Bi_{0.03}Co_{1.9}As_2$ at low temperatures. The values of the local magnetic fields of 2.59(2) T and 5.92(1) T on ^{139}La and ^{75}As nuclei, respectively, were determined in the magnetically ordered state. A strong reduction of the local magnetic field on ^{59}Co nuclei in the vicinity of Bi defects was observed.

Electronic Structure. Nonpolarized electronic band structures of $LaCo_2As_2$ and $PrCo_2As_2$ were calculated using the LMTO approach to elucidate the origin of magnetic ordering. The calculations were performed on idealized crystal structures, without inclusion of Bi defect sites or Co vacancies. The nonmagnetic calculations revealed a very strong peak in the density of states (DOS) at the Fermi level, mainly arising from the contribution of the Co 3d orbitals (Figure 15, top). Approximating the Co−Co exchange interaction (J) by the value reported for the free Co metal,[35] we find that the value of DOS at the Fermi level, $n(E_F)$, allows the satisfaction of the Stoner criterion for itinerant ferromagnetism, $J\cdot n(E_F) > 1$.[36] The results of DFT calculations lead to $J\cdot n(E_F)$ of 2.1 and 2.0 for $LaCo_2As_2$ and $PrCo_2As_2$, respectively. A criterion proposed by Dronskowski suggests the need for strong antibonding interactions at the Fermi level as the driving force for the FM ordering.[37] Indeed, the crystals orbital Hamilton population (COHP) analysis of the Co−Co bonding in $LaCo_2As_2$ and $PrCo_2As_2$ reveals the strong antibonding character of Co−Co interactions in the $[Co_2As_2]$ layer (Figure 15, bottom), thus satisfying the Dronskowski's criterion and supporting the FM ordering observed experimentally.

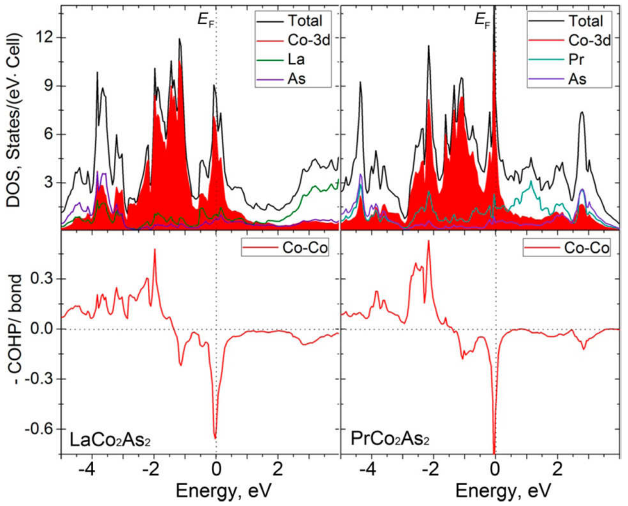

Figure 15. Density of states (DOS, top) and Co−Co crystal orbital Hamilton population (COHP, bottom) plots for $LaCo_2As_2$ (left) and $PrCo_2As_2$ (right). The individual contribution of each element to the total DOS is shown. The contribution from the Co 3d orbitals is emphasized with red shading. The positive and negative values of −COHP indicate the bonding and antibonding Co−Co interactions, respectively.

The spin-polarized band structure calculations were performed on the idealized structures of $LaCo_2As_2$ and $PrCo_2As_2$ using the FPLO code. The strong polarization of the Co 3d subband (Figure 16) is consistent with the itinerant FM ordering. The calculations resulted in the expected magnetic moment of 0.75 μ_B per Co atom in on $LaCo_2As_2$, which is in reasonable agreement with the measured value of 0.59 μ_B at 1.8 K. For $PrCo_2As_2$, the calculation was based on a FiM ground state model in which the Pr and Co moments were set antiparallel to each other. The calculated magnetic moment of Pr (2.1 μ_B) was lower than the theoretically expected value (3.2 μ_B), while the calculated Co moment (0.75 μ_B) was higher than the value obtained from the field-dependent magnetization at 30 K (0.37 μ_B). This discrepancy suggests that our calculations might have certain shortcomings, especially with regard to the treatment of 4f magnetism for the Pr^{3+} ions with the strong spin−orbit coupling, as well as that the real magnetic structure might be more complicated than the simple FiM model. One also should keep in mind that the calculations were performed for the idealized structures of $LaCo_2As_2$ and $PrCo_2As_2$, but the presence of Co vacancies, undoubtedly, influences the crystal orbital populations and the spin polarization at E_F.

■ CONCLUDING REMARKS

This work establishes Bi flux as an effective reaction medium for the synthesis of ternary arsenides, RCo_2As_2 (R = La−Nd). The X-ray crystal structure determination reveals the formation of Co vacancies in all these materials, as well as the incorporation of Bi defects into the structures of La- and Ce-containing phases, leading to the general formula

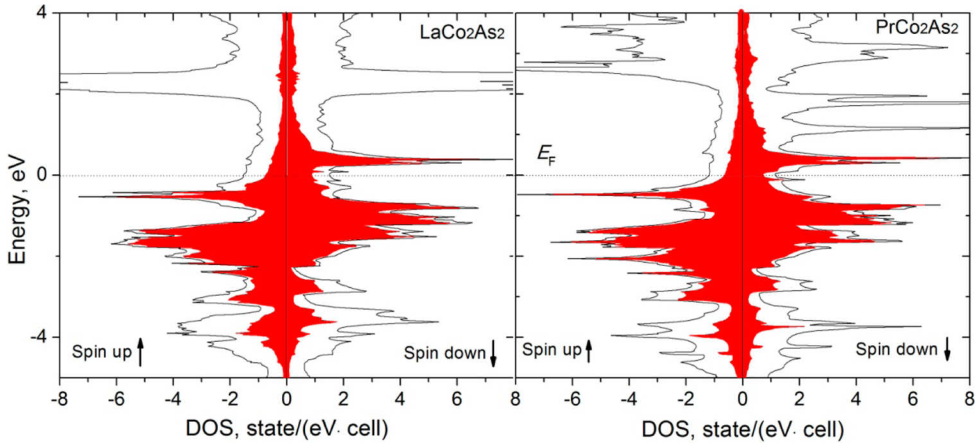

Figure 16. Spin-polarized DOS for $LaCo_2As_2$ (left) and $PrCo_2As_2$ (right). The red-shaded area indicates the contribution of the Co 3*d* orbitals.

$R_{1-x}Bi_xCo_{2-\delta}As_2$. The formation of Co vacancies was also confirmed by EDX microanalysis and Rietveld structural refinement from neutron powder diffraction data. All compounds exhibit ferromagnetic (FM) ordering of Co magnetic moments at higher temperature. Magnetic studies on single crystals show that the Co moments align along the tetragonal *c* axis. At lower temperatures, the rare-earth magnetic moments (for R = Ce, Pr, Nd) order antiparallel to the Co moments, stabilizing a ferrimagnetic (FiM) ground state. The NMR spectroscopy performed on $La_{0.97}Bi_{0.03}Co_{1.9}As_2$ provides the values of the local magnetic fields of 2.59(2) T and 5.92(1) T on the ^{139}La and ^{75}As nuclei, respectively, in the magnetically ordered state. We also observed a strong reduction of the local magnetic field on the ^{59}Co nuclei in the vicinity of Bi defects. Interestingly, the Pr- and Nd-containing samples are likely antiferromagnetic (AFM) at the lowest temperature of our experiments, as the magnetization measurements at 1.8 K revealed two consecutive metamagnetic transitions. Further studies, employing polarized neutron diffraction and X-ray magnetic circular dichroism spectroscopy, will be performed in the future to shed light on the field-dependent behavior and magnetically ordered structures of $Ce_{0.95}Bi_{0.05}Co_{1.85}As_2$, $PrCo_{1.8}As_2$, and $NdCo_{1.7}As_2$.

We note that the magnetic behavior of RCo_2As_2 is quite different from that established for the isostructral phosphides, RCo_2P_2. All the RCo_2As_2 materials exhibit FM ordering of Co 3*d* moments along the *c* axis, while among the corresponding phosphides only $LaCo_2P_2$ shows FM ordering of Co moments, which are aligned parallel to the *ab* plane. All the other RCo_2P_2 phases exhibit AFM ordering in the Co sublattice near or above the room temperature and AFM ordering in the R sublattice below 20 K.[8] Thus, the 3*d* and 4*f* magnetic orderings are "decoupled" in RCo_2P_2 because of the cancellation of Co moments at rather high temperatures. In contrast, the FM ordering of Co moments in RCo_2As_2 allows the observation of the 3*d*-4*f* coupling effects in these materials. Especially interesting is the fact that this 3*d*-4*f* exchange is AFM in nature, resulting in FiM ground states for R = Ce, Pr, and Nd. This situation is in drastic contrast to the well-established properties of related layered binary structures, RCo_2, in which the 3*d* and 4*f* moments are always coupled FM for the lighter lanthanides.[38] Therefore, our findings indicate that the nonmetal atoms should play a significant role in defining the character of magnetic exchange interactions in RCo_2As_2. Undoubtedly, further experimental and theoretical studies are required to better understand the nature and mechanisms of the magnetic phase transitions observed in these materials.

■ ASSOCIATED CONTENT

Ⓢ Supporting Information

Figures S1−S10. Table S1. CIF files. This material is available free of charge via the Internet at http://pubs.acs.org.

■ AUTHOR INFORMATION

Corresponding Author

*Email: shatruk@chem.fsu.edu.

Notes

The authors declare no competing financial interest.

■ ACKNOWLEDGMENTS

This research is supported by the National Science Foundation CAREER Award to M.S. (DMR-0955353). The work at the Oak Ridge National Laboratory was sponsored by the Scientific User Facilities Division, Office of Basic Energy Sciences, U.S. Department of Energy (DOE). The authors also acknowledge Helmholtz-Zentrum Berlin for providing the beamtime at experimental station of BESSY-II storage ring. A.Y. and A.M. thank the Russian Scientific Foundation for support. A.A.G., N.B., and W.K. were supported by the Deutsche Forschungsgemeinschaft (DFG) via TRR 80 (Augsburg, Munich, Stuttgart).

■ REFERENCES

(1) (a) Rotter, M.; Pangerl, M.; Tegel, M.; Johrendt, D. *Angew. Chem., Int. Ed.* **2008**, *47*, 7949. (b) Saha, S. R.; Butch, N. P.; Drye, T.; Magill, J.; Ziemak, S.; Kirshenbaum, K.; Zavalij, P. Y.; Lynn, J. W.; Paglione, J. *Phys. Rev. B* **2012**, *85*, 024525. (c) Zapf, S.; Wu, D.; Bogani, L.; Jeevan, H. S.; Gegenwart, P.; Dressel, M. *Phys. Rev. B* **2011**, *84*, 140503. (d) Saha, S. R.; Butch, N. P.; Kirshenbaum, K.; Paglione, J.; Zavalij, P. Y. *Phys. Rev. Lett.* **2009**, *103*, 037005.

(2) Rotter, M.; Tegel, M.; Johrendt, D. *Phys. Rev. Lett.* **2008**, *101*, 107006.

(3) Sefat, A. S.; Jin, R.; McGuire, M. A.; Sales, B. C.; Singh, D. J.; Mandrus, D. *Phys. Rev. Lett.* **2008**, *101*, 117004.

(4) Sefat, A. S.; Singh, D. J.; Jin, R.; McGuire, M. A.; Sales, B. C.; Mandrus, D. *Phys. Rev. B* **2009**, *79*, 024512.

(5) Pandey, A.; Quirinale, D. G.; Jayasekara, W.; Sapkota, A.; Kim, M. G.; Dhaka, R. S.; Lee, Y.; Heitmann, T. W.; Stephens, P. W.; Ogloblichev, V.; Kreyssig, A.; McQueeney, R. J.; Goldman, A. I.; Kaminski, A.; Harmon, B. N.; Furukawa, Y.; Johnston, D. C. *Phys. Rev. B* **2013**, *88*, 014526.

(6) (a) Cheng, B.; Hu, B. F.; Yuan, R. H.; Dong, T.; Fang, A. F.; Chen, Z. G.; Xu, G.; Shi, Y. G.; Zheng, P.; Luo, J. L.; Wang, N. L. *Phys. Rev. B* **2012**, *85*, 144426. (b) Ying, J. J.; Yan, Y. J.; Wang, A. F.; Xiang, Z. J.; Cheng, P.; Ye, G. J.; Chen, X. H. *Phys. Rev. B* **2012**, *85*, 214414.

(7) Ballinger, J.; Wenger, L. E.; Vohra, Y. K.; Sefat, A. S. *J. Appl. Phys.* **2012**, *111*, 07E106.

(8) (a) Mörsen, E.; Mosel, B. D.; Müller-Warmuth, W.; Reehuis, M.; Jeitschko, W. *J. Phys. Chem. Solids* **1988**, *49*, 785. (b) Reehuis, M.; Jeitschko, W. *J. Phys. Chem. Solids* **1990**, *51*, 961.

(9) Kovnir, K.; Thompson, C. M.; Zhou, H. D.; Wiebe, C. R.; Shatruk, M. *Chem. Mater.* **2010**, *22*, 1704.

(10) Kovnir, K.; Thompson, C. M.; Garlea, V. O.; Haskel, D.; Polyanskii, A. A.; Zhou, H. D.; Shatruk, M. *Phys. Rev. B* **2013**, *88*, 104429.

(11) Kovnir, K.; Garlea, V. O.; Thompson, C. M.; Zhou, H. D.; Reiff, W. M.; Ozarowski, A.; Shatruk, M. *Inorg. Chem.* **2011**, *50*, 10274.

(12) Marchand, R.; Jeitschko, W. *J. Solid State Chem.* **1978**, *24*, 351.

(13) Thompson, C. M.; Kovnir, K.; Eveland, S.; Herring, M. J.; Shatruk, M. *Chem. Commun.* **2011**, *47*, 5563.

(14) Akselrud, L. G.; Zavalii, P. Y.; Grin, Y.; Pecharski, V. K.; Baumgartner, B.; Woelfel, E. *Mater. Sci. Forum* **1993**, *133−136*, 335.

(15) *SMART and SAINT*. Bruker AXS Inc.: Madison, WI, 2007.

(16) Sheldrick, G. M. *Acta Crystallogr., Sect. A* **2008**, *A64*, 112.

(17) Garlea, V. O.; Chakoumakos, B. C.; Moore, S. A.; Taylor, G. B.; Chae, T.; Maples, R. G.; Riedel, R. A.; Lynn, G. W.; Selby, D. L. *Appl. Phys. A: Mater. Sci. Process.* **2010**, *99*, 531.

(18) Rodríguez-Carvajal, J. *Physica B* **1993**, *192*, 55.

(19) (a) Koepernik, K.; Eschrig, H. *Phys. Rev. B* **1999**, *59*, 1743. (b) Opahle, I.; Koepernik, K.; Eschrig, H. *Phys. Rev. B* **1999**, *60*, 14035.

(20) Perdew, J. P.; Wang, Y. *Phys. Rev. B* **1992**, *45*, 13244.

(21) Tank, R.; Jepsen, O.; Burkhardt, A.; Andersen, O. K. *The Program TB-LMTO-ASA. Version 4.7.* Max-Planck-Institut fur Festkorperforschung: Stuttgart, 1999.

(22) Von Barth, U.; Hedin, L. *J. Phys. C* **1972**, *5*, 1629.

(23) Blochl, P. E.; Jepsen, O.; Andersen, O. K. *Phys. Rev. B* **1994**, *49*, 16223.

(24) Okamoto, H. *Desk Handbook: Phase Diagrams for Binary Alloys*. 2nd ed.; ASM International: Materials Park, OH, 2010; p 855. We note, however, that the very first Co-Bi binary compound, $CoBi_3$, has been discovered recently:. Schwarz, U.; Tencé, S.; Janson, O.; Koz, C.; Krellner, C.; Burkhardt, U.; Rosner, H.; Steglich, F.; Grin, Y. *Angew. Chem., Int. Ed.* **2013**, *52*, 9853.

(25) (a) Bukowski, Z.; Weyeneth, S.; Puzniak, R.; Moll, P.; Katrych, S.; Zhigadlo, N. D.; Karpinski, J.; Keller, H.; Batlogg, B. *Phys. Rev. B* **2009**, *79*, 104521. (b) Mathieu, J. L.; Latturner, S. E. *Chem. Commun.* **2009**, 4965.

(26) (a) El Ghadraoui, E. H.; Pivan, J. Y.; Guerin, R.; Pena, O.; Padiou, J.; Sergent, M. *Mater. Res. Bull.* **1988**, *23*, 1345. (b) Stoyko, S. S.; Blanchard, P. E. R.; Mar, A. *J. Solid State Chem.* **2012**, *194*, 113. (c) Bobev, S.; Xia, S.; Bauer, E. D.; Ronning, F.; Thompson, J. D.; Sarrao, J. L. *J. Solid State Chem.* **2009**, *182*, 1473.

(27) (a) Geller, S.; Williams, H. J.; Espinosa, G. P.; Sherwood, R. C.; Gilleo, M. A. *Appl. Phys. Lett.* **1963**, *3*, 21. (b) Hansen, P.; Witter, K.; Tolksdorf, W. *Phys. Rev. B* **1983**, *27*, 4375.

(28) Sanderson, R. T. *Chemical Bonds and Bond Energy*, 2nd ed.; Academic Press: 1976; 224 pp.

(29) Reehuis, M.; Ritter, C.; Ballou, R.; Jeitschko, W. *J. Magn. Magn. Mater.* **1994**, *138*, 85.

(30) Reehuis, M.; Jeitschko, W.; Kotzyba, G.; Zimmer, B.; Hu, X. *J. Alloys Compd.* **1998**, *266*, 54.

(31) (a) Néel, L. *Ann. Phys.* **1948**, *3*, 137. (b) Pauthenet, R. *J. Appl. Phys.* **1958**, *29*, 253. (c) Mathonière, C.; Nuttall, C. J.; Carling, S. G.; Day, P. *Inorg. Chem.* **1996**, *35*, 1201. (d) Ohkoshi, S. i.; Hashimoto, K. *J. Am. Chem. Soc.* **1999**, *121*, 10591. (e) Egan, L.; Kamenev, K.; Papanikolaou, D.; Takabayashi, Y.; Margadonna, S. *J. Am. Chem. Soc.* **2006**, *128*, 6034.

(32) Reehuis, M.; Brown, P. J.; Jeitschko, W.; Möller, M. H.; Vomhof, T. *J. Phys. Chem. Solids* **1993**, *54*, 469.

(33) Gippius, A. A.; Gervits, N. E.; Tkachev, A. V.; Maslova, I. S.; Volkova, O. S.; Vasiliev, A. N.; Büttgen, N.; Krätschmer, W.; Moskvin, A. S. *Phys. Rev. B* **2012**, *86*, 155114.

(34) Büttgen, N.; Bohmer, R.; Krimmel, A.; Loidl, A. *Phys. Rev. B* **1996**, *53*, 5557.

(35) Janak, J. F. *Phys. Rev. B* **1977**, *16*, 255.

(36) Stoner, E. C. *Proc. R. Soc. Ser. A* **1938**, *165*, 372.

(37) Landrum, G. A.; Dronskowski, R. *Angew. Chem., Int. Ed.* **2000**, *39*, 1560.

(38) Duc, N. H.; Brommer, P. E. *Handb. Magn. Mater.* **1999**, *12*, 259.